Reliability of self-affine measurements

Jean Schmittbuhl and Jean-Pierre Vilotte
Département T.A.O., Laboratoire de Géologie, URA 1316, École Normale Supérieure, 24 rue Lhomond, 75231 Paris cedex 05, France

Stéphane Roux
Laboratoire de Physique et Mécanique des Milieux Hétérogènes, URA 857, École Supérieure de Physique et Chimie Industrielles, 10 rue Vauquelin, 75231 Paris cedex 05, France

(Received 12 April 1994)

Reliability and accuracy of the determination of self-affine exponents are studied and quantified from the analysis of synthetic self-affine profiles and surfaces. The self-affine exponent is measured using different methods either relying on the determination of a "fractal dimension" (i.e., box counting and divider methods) or directly analyzing the self-affine exponent. The second group of methods includes the variable bandwidth, the first return and the multireturn probability distribution, and the power spectrum. The accuracy of all these methods is assessed in terms of the difference between an "input" self-affine exponent used for the synthetic construction and the "output" exponent measured by those different methods. The statistical results of this study provide a quantitative estimate of the dependence of the accuracy with the system size and the value of the self-affine exponent. Artifacts in the measurement of self-affine profiles or surfaces, misorientation, signal amplification, and local geometric filtering, which lead to biased estimates of the self-affine exponent, are also discussed.

PACS number(s): 05.40.+j, 68.35.Bs, 61.43.Hv, 47.53.+n

I. INTRODUCTION

In recent years the descriptions of scaling invariance have become of crucial importance for many physical problems. The concept of self-similarity, e.g., developed by Mandelbrot [1], has been extended to account for anisotropy through the notion of *self-affine* symmetry. This scaling is fully characterized by $d-1$ exponents in d-dimensional space. For $d=2$ (e.g., two-dimensional cuts such as the one considered in the body of this paper), one single exponent is needed. It is called the *Hurst,* or self-affine, exponent. A large number of natural surfaces are found to be self-affine, such as those encountered in surface growth models [2], in landscape and erosion surfaces [3], or in fracture surfaces [4–8].

Most of the methods used for the determination of a self-affine invariance are devoted to $(1+1)$-dimensional profiles and their reliability has hardly ever been discussed [8–11]. When it is, accuracy is only meant as an estimate of the quality of the power-law regression. In particular, no systematic comparison of the different analysis tools is available.

Methods for measuring self-affine exponents can be schematically cast into two groups. On the one hand, one finds the classical methods, developed for analyzing self-similar objects: divider method, box counting method, area-perimeter method, etc., which provide a so-called "fractal dimension." For most of these methods, a relationship with the self-affine exponent has been derived. On the other hand, several methods have been designed to specifically determine the self-affine exponent. They are more recent and not always systematically documented.

A number of artifacts may "pollute" the measurement of a self-affine object and hence introduce systematic errors in the self-affine exponent. Two types of biases can be distinguished: those which take place during the geometric measurement of the object and those which are relative to the method used in the signal analysis. In the latter case, sensitivity and accuracy are method dependent, and from the results reported below, we strongly recommend the simultaneous use of different tools in order to appreciate the confidence in the measured exponent in a quantitative way.

An accurate estimation of the self-affine exponent may have deep physical implications and is of crucial importance for the identification of the universality class of various phenomena such as fracture propagation [5,7,12]. Fracture surfaces are found to be self-affine with a well defined exponent quite insensitive to the material type and the rupture mode. Whenever this observation is violated, one may wonder whether it is a real violation or simply a systematic underestimation of error bars in the analysis. This point may also help to resolve apparent discrepancies in published results. The existence of some universal symmetries of the fracture propagation process is an exciting problem which heavily relies on an accurate and faithful analysis of experimental data.

Another example where the role of the analyzing tools in self-affine measurement is crucial is a recent very active debate on the roughness of imbibition fronts in a porous medium. The reported experimental values were all inconsistent with most available models. A recent analysis [13] shows that a possible origin of this discrepancy—or even more annoyingly, of apparent agreement between different studies—may result from a

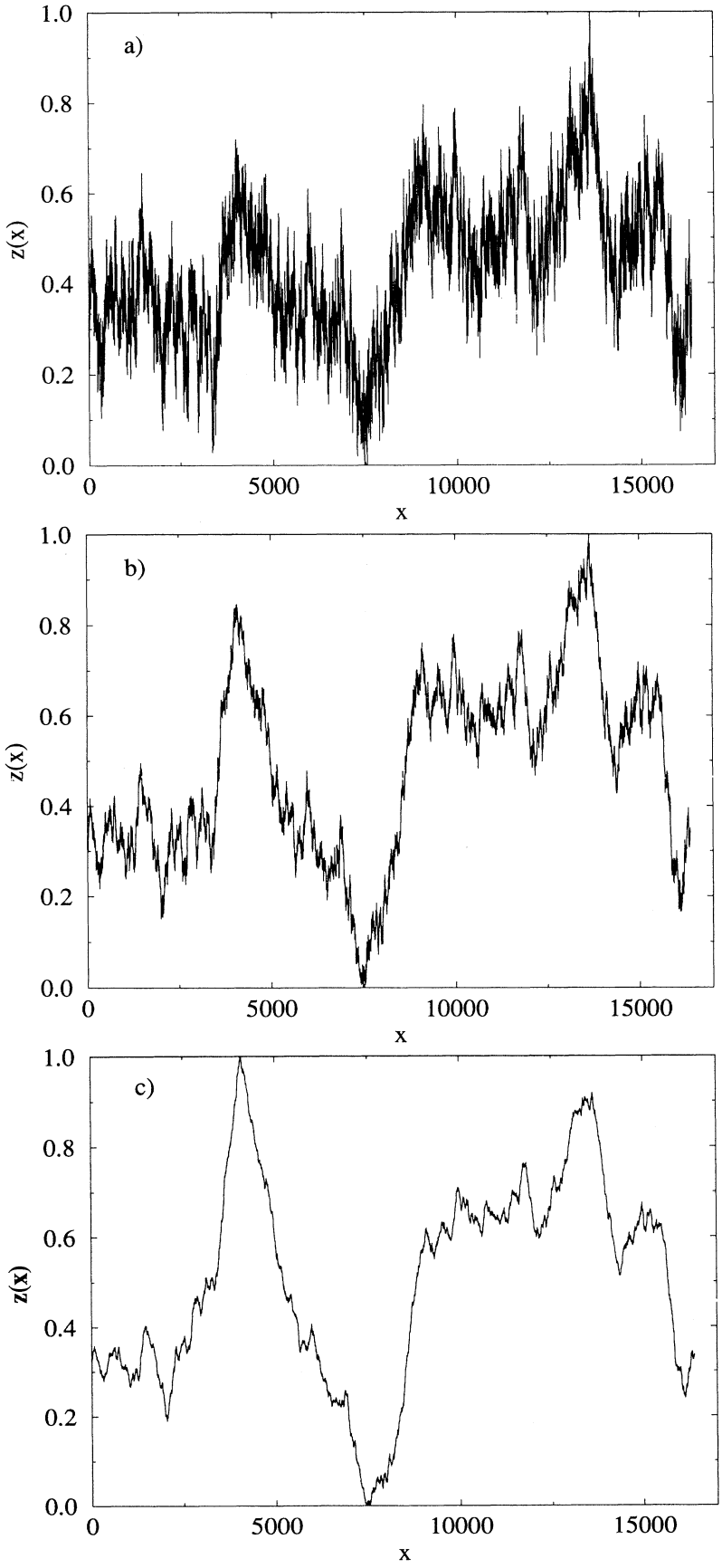

FIG. 1. Three examples of synthetic self-affine profiles for different self-affine exponents, respectively, (a) $\zeta=0.2$, (b) $\zeta=0.5$, and (c) $\zeta=0.8$.

misuse of a measurement technique out of its field of validity.

In order to assess the accuracy and the reliability of the different methods of signal processing, these are tested against synthetic self-affine sets considered here as "ideal" and which are well characterized by a prescribed self-affine exponent. Artificial alterations of the profiles corresponding to what could be measurement biases have also been introduced in order to estimate their influence on the exponent determination. Other effects such as the existence of a crossover at intermediate length scales or multifractal properties are not considered in this study. One should keep in mind that the analysis presented here addresses only "monofractal" objects [14]. Multifractal signals where the Hurst exponent becomes ill defined (it depends on the order of the studied moments) are not considered.

This paper is organized as follows. In Sec. II, self-affine properties are briefly reviewed and the generation procedure of the synthetic sets is presented. In Sec. III, we consider the tools derived from the techniques initially developed for self-similar objects and which provide a fractal dimension. In Sec. IV independent methods for the self-affine characterization are described. Section V is devoted to the systematic study of the accuracy of those methods. Finally, in Sec. VI, the influence of some of the most important measurement artifacts on the self-affine analysis is investigated.

II. SELF-AFFINE PROFILE CONSTRUCTION

A self-affine set is statistically invariant under an affine transformation. For a horizontal surface, the affine transformation is written in terms of the horizontal distances d_x and d_y and the vertical distance d_z

$$d_x \rightarrow \lambda_x d_x, \quad d_y \rightarrow \lambda_y d_y, \quad d_z \rightarrow \lambda_z d_z \ . \tag{2.1}$$

Requiring that such transformations can be combined implies a group structure. As a consequence, λ_y and λ_z have to be homogeneous functions of, say, λ_x. The homogeneity exponents are called the *self-affine exponents,* or Hurst exponents. They obey

$$\lambda_y = \lambda_x^{\zeta_y}, \quad \lambda_z = \lambda_x^{\zeta_z} \ . \tag{2.2}$$

Isotropy along the (x,y) plane implies $\zeta_y = 1$. In this study, we will restrict ourselves to the two-dimensional case where a single ζ exponent is needed. These two-dimensional sets can always be considered as cuts through a three-dimensional medium. Conventionally, we assume that the profile lies in the (x,z) plane.

Ideal self-affine objects are constructed using the algorithm proposed by Voss [15]. For $(1+1)$-dimensional profiles the basic procedure is as follows: knowing the values of z at both ends i and j of a root segment, we compute its value at the center l as the average $(z_i + z_j)/2$ plus a fluctuation $\alpha\epsilon$. At each generation k, the fluctuation ϵ_k is picked from a statistical distribution $f(\epsilon)$ with zero mean and scaled by a factor α proportional to the length of the parent segment $|i-j|$ raised to the power ζ, ζ being the prescribed self-affine exponent. The distribution f can be chosen, without any loss of generality, to be a Gaussian distribution. Figures 1(a), 1(b), and 1(c) show examples of such self-affine profiles for, respectively, three different exponents: 0.2, 0.5, and 0.8, each of them being normalized so that the maximum magnitude of the signal is identical for all profiles.

For this study, each profile is characterized by both a self-affine exponent ζ and a size L. We systematically analyze profiles with an exponent in the range [0.1,0.9] with a step of 0.1 and system sizes in geometrical series from 2^5 to 2^{14}. For each point of the space (ζ, L), a set of 100 independent profiles is considered.

III. MEASUREMENT OF FRACTAL DIMENSION

One of the most often used methods to characterize a self-affine structure is to estimate the fractal dimension of the profile. Although it seems natural to associate a fractal dimension with an object that fulfills some kind of scale invariance, it has been recognized for a long time that the very concept of fractal dimension is not well defined as soon as the symmetry obeyed by the structure is not a pure self-similarity.

The reason for such a statement is that the fractal dimension gives the scaling of a measure with a length scale. For a self-affine object, the scaling with the distance along one axis may differ depending on the orientation of the axis. We will see below that a variety of different fractal dimensions can be defined and observed.

The vague definition of a fractal dimension for a self-affine object has, in the past, resulted in some misuse of the fractal dimension in this framework, as well as some confusion in the measure of this property. Nevertheless, we will analyze two methods which have been introduced in this connection and used in the past: the *box counting* and the *divider* method.

A. The box counting method

The box counting method consists of covering the profile with boxes of size $a \times (\mu a)$ for a fixed aspect ratio μ and various sizes a. Let $n(a)$ be the number of boxes needed to cover the profile. We can estimate the scaling of $n(a)$ for a profile such that $\langle \Delta z \rangle = A \Delta x^{\zeta}$, where A is the amplitude of the profile. Over a distance $\Delta x = a$, the fluctuation of height amounts to $\Delta z = A a^{\zeta}$. Two situations can arise: if $A a^{\zeta} \gg \mu a$, then the number of boxes to consider in the interval $[x, x+a]$ will be $A/\mu a^{\zeta-1}$, so that the total number of boxes over a profile of length L_x will be

$$n(a) = (A/\mu) L_x a^{\zeta-2} \quad \text{for } a \ll (A/\mu)^{1/(1-\zeta)} \ . \tag{3.1}$$

On the other hand, if $A a^{\zeta} \leq \mu a$, the number of boxes will be one over a distance a along x. Thus, in this case the total number of boxes can simply be expressed as

$$n(a) = L_x a^{-1} \quad \text{for } a \geq (A/\mu)^{1/(1-\zeta)} \ . \tag{3.2}$$

Thus the roughness exponent ζ can only be measured in a specific range of a values. Moreover, it should be noted that the upper bound on a depends on the aspect ratio of the box μ or, alternatively, on the amplitude of the profile

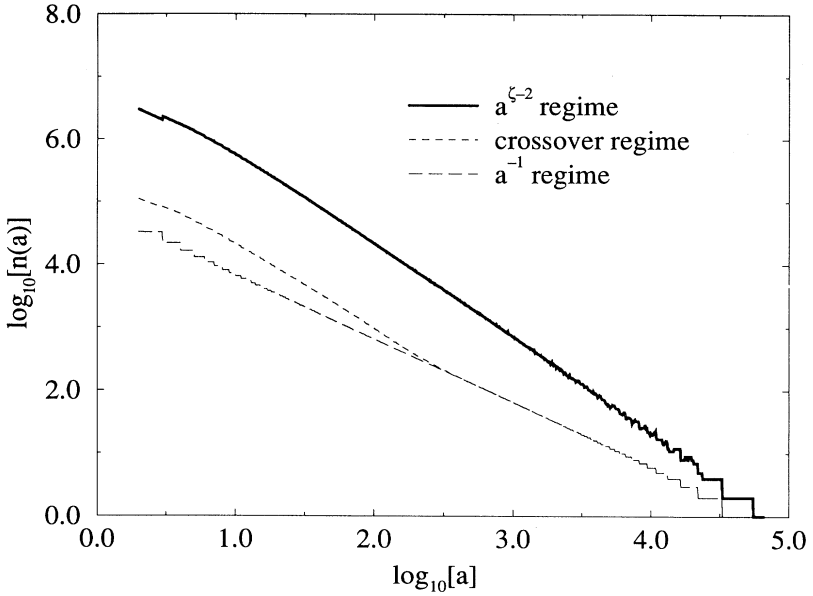

FIG. 2. Analysis of a synthetic profile of length 65 536 with a 0.5 exponent by the box counting method. The decimal logarithm of the number of boxes $n(a)$ is plotted according to the box length a. According to the height of boxes, two kinds of regimes are expected.

A. This upper bound does not mean that the correlations have died over this distance. It is an intrinsic limitation of the method and does not reveal a correlation distance. Therefore, in order to use this method, one should be careful in setting the parameter μ, or rather one should perform the measurement for different values of μ.

In Fig. 2 we show the evolution of $n(a)$ vs a for three different μ. One corresponds to the regime (3.1), another to the other regime (3.2), and a third one displays a crossover between both regimes at an intermediate length scale.

We can derive a simple property from the above results which will be useful in the following discussion. For μ small enough to be in the regime (3.1), we consider a strip $z_0 < z < z_0 + \mu a$ for a z_0 such that the profile is intersected at least once. The number of possible strips satisfying this property is $n_s = AL_x^{\zeta}/(\mu a)$. Assuming that each strip is equivalent, we can compute the number of boxes per strip

$$n_x = n(a)/n_s = \left[\frac{L_x}{a}\right]^{1-\zeta} . \tag{3.3}$$

We see that the aspect ratio μ does not appear in the expression of n_x. Thus as μ tends to zero, the strip tends to a line, and for each line, we are measuring—using a box counting technique—the fractal dimension of the intersection between the line and the profile. This fractal dimension can be read from Eq. (3.3) as $D_1 = 1-\zeta$.

B. The divider method

We now turn to another method which appears to be close to the previous one, although it gives rather different information. The *divider* method consists of computing the length of the profile by walking a yardstick of length a over it. Again, one computes the number of intersections $n(a)$ vs a. Let us first derive the expected scaling behavior and then discuss its validity. The two end points of the yardstick at a given stage are such that $a^2 = \Delta x^2 + \Delta z^2$. Therefore one should distinguish two regimes: one for which $\Delta x \gg \Delta z$ and one for which the opposite inequality holds. As in the previous method, both regimes can be encountered depending on the yardstick length a.

If $\Delta x \ll \Delta z$, then $\Delta z \approx a$, and since $\Delta z = A\,\Delta x^{\zeta}$, we can write $\Delta x \approx (a/A)^{1/\zeta}$. Therefore,

$$n(a) = L_x \left[\frac{a}{A}\right]^{-1/\zeta} \quad \text{for} \quad a \ll A^{1/(1-\zeta)} . \tag{3.4}$$

If $\Delta x \gg \Delta z$, then $\Delta x \approx a$. The expression of $n(a)$ is thus similar to Eq. (3.2), but for a slightly different condition,

$$n(a) = L_x a^{-1} \quad \text{for} \quad a \gg A^{1/(1-\zeta)} . \tag{3.5}$$

Figure 3 shows a typical measurement of $n(a)$ for a large profile changing the amplitude A to cross from the first regime (3.4) to the second regime (3.5). The theoretical slope for the self-affine sensitive regime is indicated by a thin line. We indeed observe good agreement for a large yardstick length, but at a smaller scale, strong corrections are observed.

The argument leading to the result (3.4) is straightforward, but it requires a more careful examination. The point is that if the value of Δz is very well defined, it is not the case for Δx. Indeed, when the magnitude of the profile is large compared to its length, so that (3.4) should hold, the ratio between extreme values of Δx becomes large (it can amount, in practice, to several orders of magnitude), although the maximum value of Δx is small compared to a. The lower bound on Δx is given by the argument developed above, provided it is larger than the short length scale cutoff, but the upper bound is not. In between the two extreme values of Δx, the probability

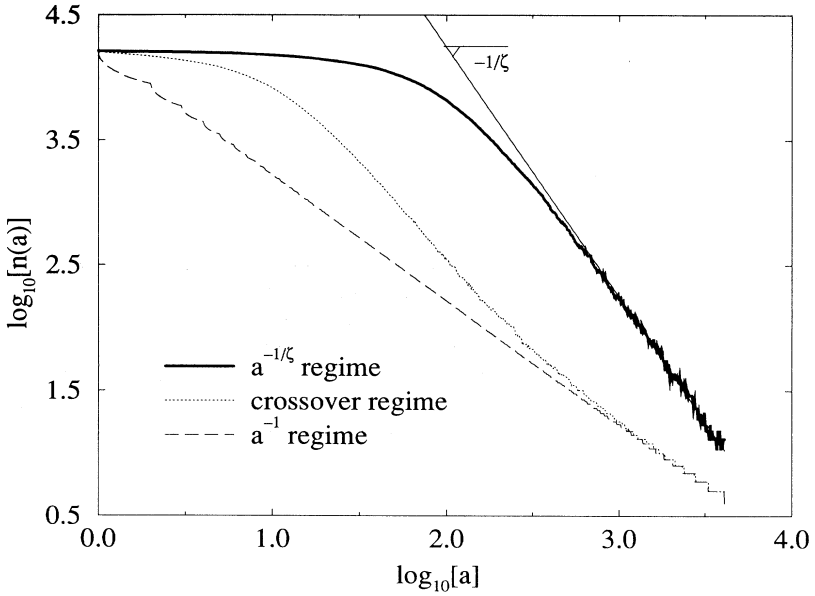

FIG. 3. Analysis of a synthetic profile of length 16 386 with a 0.5 exponent by the divider method. The decimal logarithm of the number of dividers $n(a)$ is plotted according to the divider length a. The amplitude of the signal is a very sensitive parameter and separates two distinct regimes.

distribution of Δx is a power law which can be traced back to the "first return" probability distribution (cf. Sec. IV B). In computing the number of yardsticks needed to cover the profile, only the upper bound of Δx will matter. When the yardstick length a increases, the ratio between the extreme values of Δx becomes narrower and thus the result becomes closer to the expectation (3.4). However, if a continues to increase, one will finally encounter the regime where (3.5) holds.

Let us note that a pure numerical artifact may influence the Δx distribution. Indeed, if the length Δx is considered an integer, the lower bound of the distribution is largely overestimated and the width of the distribution becomes narrow again. Subsequently, the method gets closer to the box counting method in situation (3.1). An apparent power-law regime can be found with an exponent $\zeta-2$ instead of $-1/\zeta$.

These observations lead to the conclusion that severe bounds should be imposed on the domain which allows the determination of the roughness exponent. Otherwise *any* value can be measured. This method is by far the most difficult to handle and the most restricted in range. We will, however, consider this method in Sec. V so as to prove an extensive comparison between available tools and, in particular, those which have been used in the past; however, we do not recommend the use of this method to estimate the roughness exponent. Other methods exist, in particular, in $2+1$ dimensions, such as the slit-island method [1,8], but they are not considered here.

IV. SELF-AFFINE ANALYSIS

Three independent methods for the analysis of $(1+1)$-dimensional self-affine profiles are considered here, namely, the variable bandwidth method, the return probability, and the power spectrum.

A. The variable bandwidth method

A profile of length L is divided into windows or "bands" of width Δ indexed by the position of the first point x_0 of the band. The standard deviation of the height w and the difference δ between the maximum and minimum height are computed on each band and then averaged over all the possible bands varying the origin x_0 at fixed Δ: $\langle w(\Delta)\rangle_{x_0}$ and $\langle \delta(\Delta)\rangle_{x_0}$. Bandwidths larger than $L/2$ are discarded because of insufficient independent sampling. Both quantities follow a power law of Δ, as expected for self-affine set [16]:

$$\langle w\rangle_{x_0} \propto \Delta^{\zeta}, \quad \langle \delta\rangle_{x_0} \propto \Delta^{\zeta} . \tag{4.1}$$

Figure 4 illustrates the power-law behavior of w and δ for a self-affine profile with $\zeta=0.5$.

Let us note that the variable bandwidth method is only relevant for a self-affine exponent in the range $\zeta\in[0;1]$, in agreement with the choice of exponents used for the synthetic generation of profiles. Outside this range, an apparent exponent equal to the upper or lower bound will be observed. We should note that other methods such as the spectral analysis of Sec. IV C are not limited to such a range. Therefore, when using this method, if an exponent close to 0 or 1 is detected, one should resort to the spectral analysis to check the result. Then, using the fact that a derivation reduced the self-affine exponent by one and an integration increases it by one, it is always possible to build a signal characterized by an exponent in the admissible range $\zeta\in[0;1]$ and then use the variable bandwidth method.

This method is similar to the *bridge* method [9]. The main difference is that in the latter the linear trend between the first and the last point is subtracted from the signal for each band, in contrast with the above method.

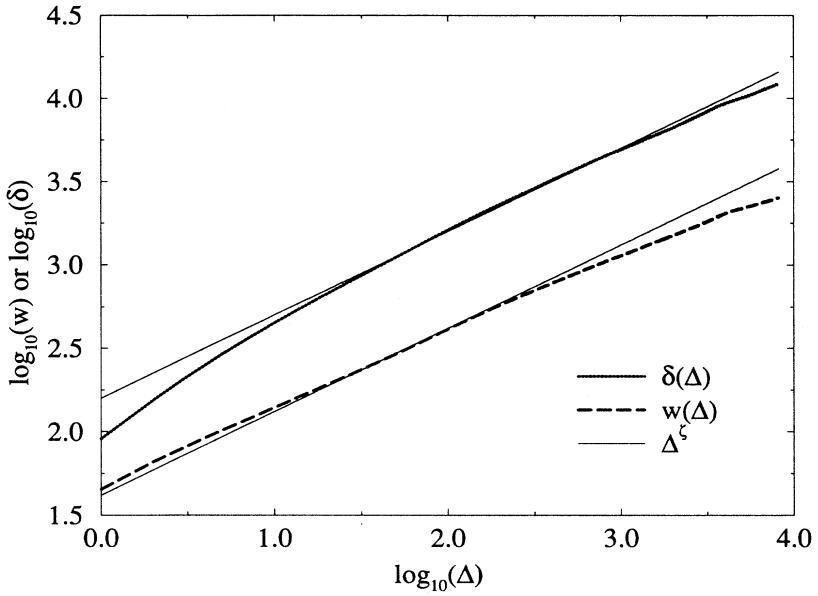

FIG. 4. Example of self-affine analyses of a synthetic profile with a 0.5 exponent by the variable bandwidth method. Estimations of the root mean square δ and the maximum-minimum difference δ, according to the bandwidth Δ, are shown. Best fits lead to the indicated value of the self-affine exponent ζ.

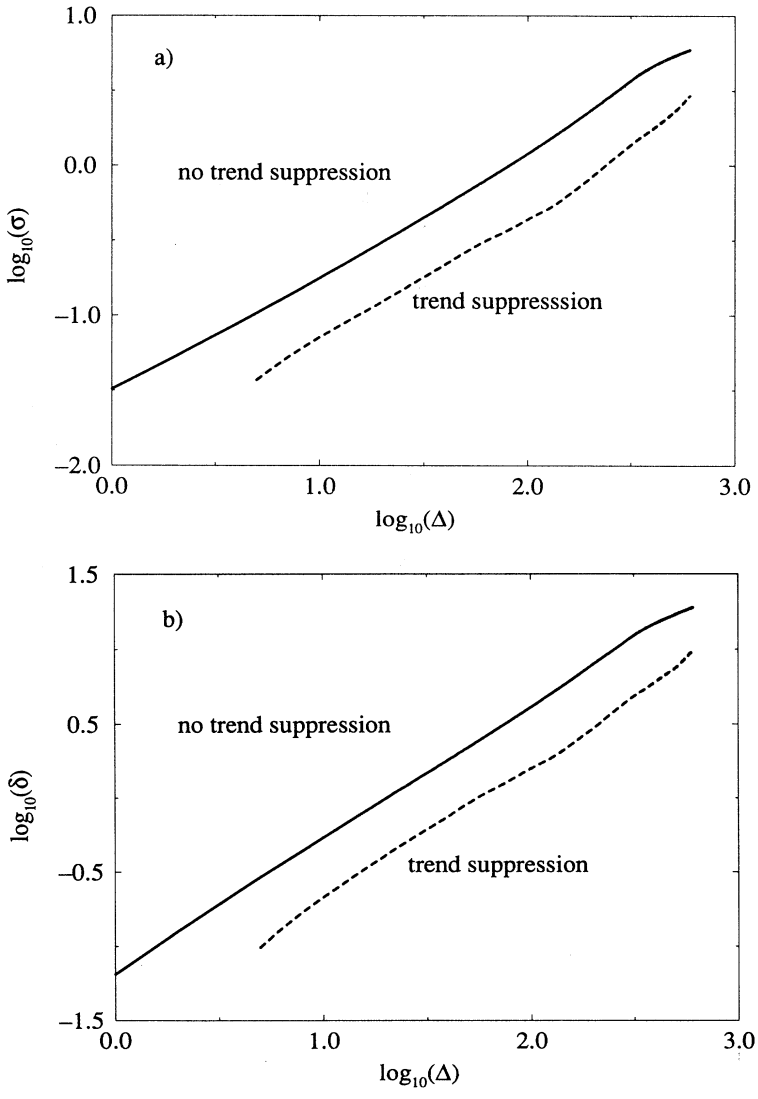

FIG. 5. Comparison of the variable bandwidth method and the *bridge* method for both estimators: (a) rms and (b) the maximum-minimum difference.

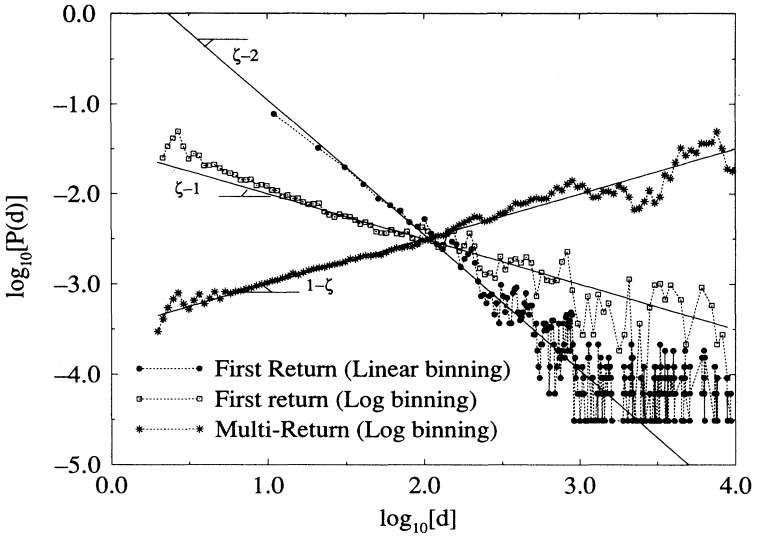

FIG. 6. Analysis of a synthetic profile of length 16 386 with a 0.5 exponent by the first return and multireturn probabilities. The return probability is the probability, starting at a given height, to cross again the profile at the same height after a distance d. When only the first intersection is considered, the method is called the first return probability. When all the intersections are considered, the method is called the multireturn probability. Actually, the probability is built as a histogram. So binning can be either linear (sizes of classes are all equal) or logarithmic.

The results of both methods are almost identical for both the rms computation [see Fig. 5(a)] and the maximum-minimum difference [see Fig. 5(b)]. This leads us to favor the variable bandwidth method since it is numerically faster.

B. Return probability

For each point x_0 of the profile with height $h(x_0)$, we see the minimum distance d at which the profile is intersected again at the same height $h(x_0+d)=h(x_0)$. The distribution of the distances d built for all the points of the profile is called the *first return* probability distribution $p_1(d)$. For self-affine profiles, it can be shown that the first return probability satisfies [17]

$$p_1(d) \propto d^{\zeta-2} . \tag{4.2}$$

This property can be derived easily from the previous discussion. We have seen above in Eq. (3.3) that the intersection between a constant height line and the profile is a fractal set of dimension $D_1=1-\zeta$. Therefore the statistical distribution of distances between intersections, and hence $p_1(d)$, follows a power law whose exponent is $-D_1-1$.

An example of this analysis is illustrated in Fig. 6 for $\zeta=0.5$. Note the poor precision that can be obtained in the curve fit due to the noise at large distances. A discussion of this technique in connection, in particular, with the effect of an additional bias is given by Hansen, Måløy, and Engøy [17].

A logarithmic binning instead of a linear one is useful to damp the fluctuations occurring for large distances. Due to the change in measure associated with a logarithmic binning, the scaling (4.2) is changed to

$$p_1^{(\log)}(d)=dp_1(d) \propto d^{\zeta-1} . \tag{4.3}$$

This is illustrated in Fig. 6.

We should also mention an alternative technique that

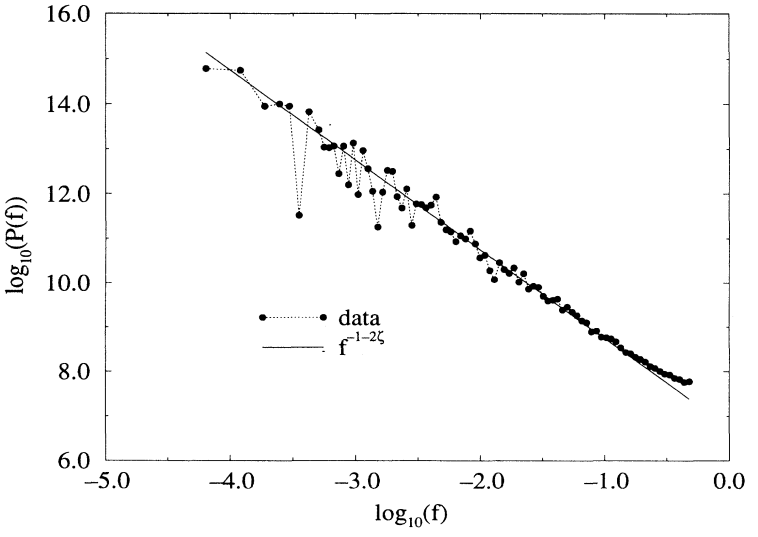

FIG. 7. Analysis of a synthetic profile of length 16 386 with a 0.5 exponent by the power spectrum method. The power $S(f)$ is plotted according to the frequency f in a decimal log-log diagram.

is related to the first return probability technique. It consists of studying the probability of *any* return—not just the first one—after a distance d. This latter probability, or *multireturn* probability, scales differently from Eq. (4.2), namely, as

$$p_m(d) \propto d^{-\zeta} . \tag{4.4}$$

This method has been used in particular by Bouchaud, Lapasset, and Planès [5].

Again this result can simply be obtained from the self-similarity of the intersection between the profile and a constant height line. Over a distance d the number of intersections scales as $N_x=(d/a)^{D_1}$ [see Eq. (3.3)]. Thus $p_m(d)$ is proportional to the derivative of n_x with respect to d. As above, a logarithmic binning of this multireturn probability scales as

$$p_m^{(\log)}(d) \propto d^{1-\zeta} . \tag{4.5}$$

Such a power law is shown in Fig. 6.

C. Power spectrum

The power spectrum $S(f)$ of the profile is the Fourier transform of the autocorrelation function $\sigma(\Delta x)=\langle h(x+\Delta x)h(x)\rangle-\langle h(x+\Delta x)\rangle\langle h(x)\rangle$. For self-affine profiles, the power spectrum is expected to scale as [18]

$$S(F) \propto f^{-1-2\zeta} . \tag{4.6}$$

This scaling result can simply be recovered by a power counting after having observed that the self-affinity implies $\sigma(\Delta x)\sim\Delta x^{2\zeta}$. Such scaling is nicely visible in Fig. 7 with a slope of -2 for an exponent $\zeta=0.5$.

V. INTRINSIC ANALYSIS ERROR BARS

Synthetic profiles of given lengths and self-affine exponents are generated as described in Sec. II. Those profiles are hereafter consider "ideal." They are analyzed with both "self-similar" methods outlined in Sec. IV—the box counting and divider methods—and "self-affine" methods—the variable bandwidth (rms and maximum-minimum difference), the first return and the multireturn probability, and the power spectrum. Their intrinsic error is defined as the difference between the *input* exponent value (used for the construction) and *output* exponent estimated from the analysis.

While the input exponent is prescribed, the output exponent is defined statistically. Indeed for each pair $(\zeta_{\text{input}}L)$, 100 analyses with the three methods are carried out from independent profiles. Then, for each method, average curves $\langle\log_{10}[n(a)]\rangle$, $\langle\log_{10}[w]\rangle$, $\langle\log_{10}(\delta)\rangle$, $\langle\log_{10}(p)\rangle$, and $\langle\log_{10}(S)\rangle$ are defined from the data. The output exponent is obtained by a linear fit of the average curves. For the box counting method, a fit is run for box sizes included in $[L/10, 9L/10]$, where L is the length of the profile. The range of meaningful divider size is much more severe especially if the self-affine exponent is small. We take care to always compute regression only in the (3.5) domain. For the variable bandwidth method, best fits are estimated when the window size is in the range $[4,3L/8]$. For the return probabilities the linear regression is in a range of distance included between 2 and half the maximum return distance. The fit for the spectral method is computed over the whole spectrum.

It should be noted that we kept the number of profiles constant, independently of the profile length, so that the data relative to the largest size represent a more significant computational effort and a broader statistical weight.

The results ζ_{output} (ζ_{input},L) for the different analysis methods are presented in two sets of plots. The first set [Figs. 8(a)–8(g)] captures the influence of the main effects: system size L and self-affinity exponent ζ_{input}. The second set [Figs. 9(a)–9(g)] focuses on the estimation of the error bars.

A. Finite size effect and self-affine exponent influence

Figures 8(a)–8(g) present a comparison between input and output exponents according to the different analysis methods. Each curve of the different graphs shows the finite size effects. The diagonal where the output exponent equals the input exponent would be the response of an ideal analyzing process.

As the system size—number of points along the profile—increases, the output exponent gets closer to the input exponent. For the first return probability method, the smallest errors are not obtained for large systems where a systematic overestimate emerges. The reason for this observation is to be found in the influence of the very noisy end of the probability distribution (see Fig. 6 as an example).

On the one hand, methods such as box counting, rms, and maximum-minimum difference are mainly sensitive to the self-affine exponent. In this case, the typical trend of the curve is not parallel to the diagonal. Small self-affine exponents are systematically overestimated whereas large exponents are underestimated. Consequently, there exists a typical value of ζ where the output exponent is correct independent of the system size. It is close to 0.4 for the rms method, 0.6 for the box counting method, and 0.7 for the maximum-minimum difference method. This leads to the global conclusion that the rms method provides generally a low value of ζ in contrast with the box counting and the maximum-minimum difference method.

On the other hand, the first return and multireturn probability methods and the power spectrum method are more sensitive to the size effects. The response is more or less parallel to the diagonal. Error is then mainly a function of the system size. The divider method shows such a behavior if we ignore the low self-affine exponent. The finite size effects are very important for the first return probability. The spectral method appears as the more accurate one with a small systematic underestimate effect.

B. Error estimates

The analysis error is defined as the difference between the input exponent and the output exponent. Figures

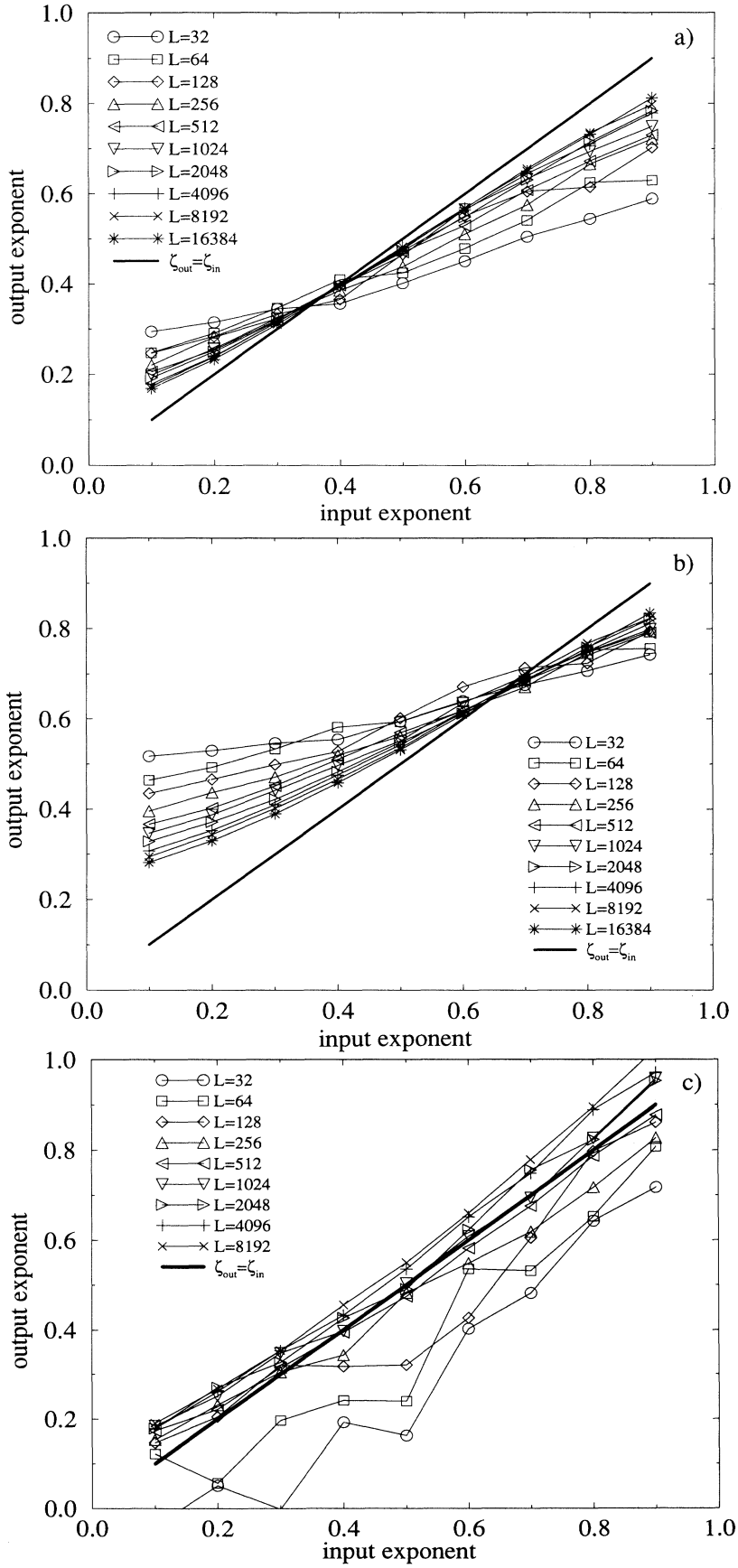

FIG. 8. Comparisons of the "output" exponent obtained from the self-affine analysis and the "input" exponent introduced in the numerical construction for the seven methods of analysis: (a) the variable bandwidth method using a rms estimator, (b) the variable bandwidth method using the maximum-minimum difference, (c) the first return probability method, (d) the multireturn probability method, (e) the power spectrum method, (f) the divider method, and (g) the box counting method. Box counting, the rms and the maximum-minimum difference are mainly sensitive to the self-affine exponent, while first return and multireturn probability and the power spectrum are more sensitive to size effects.

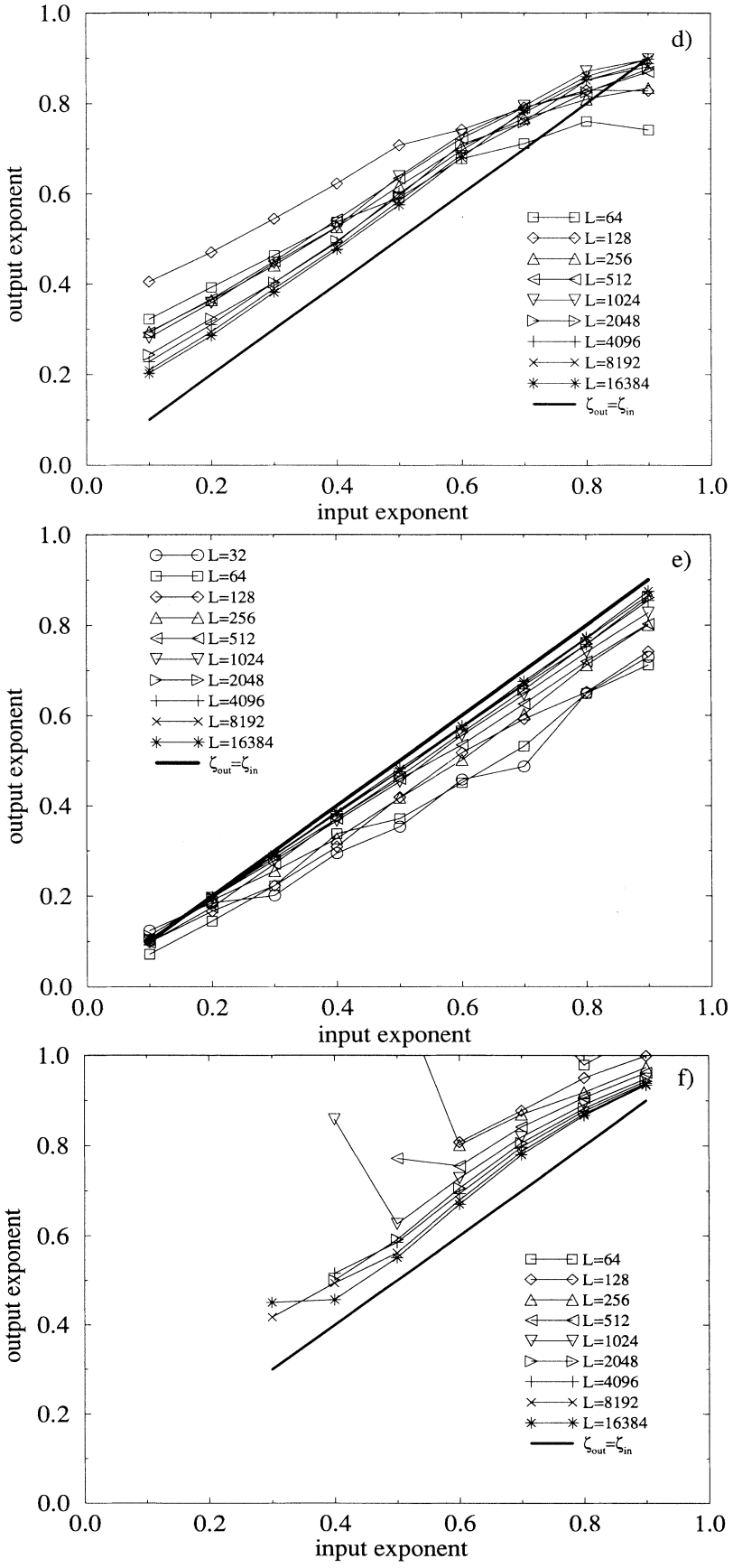

FIG. 8. (*Continued*).

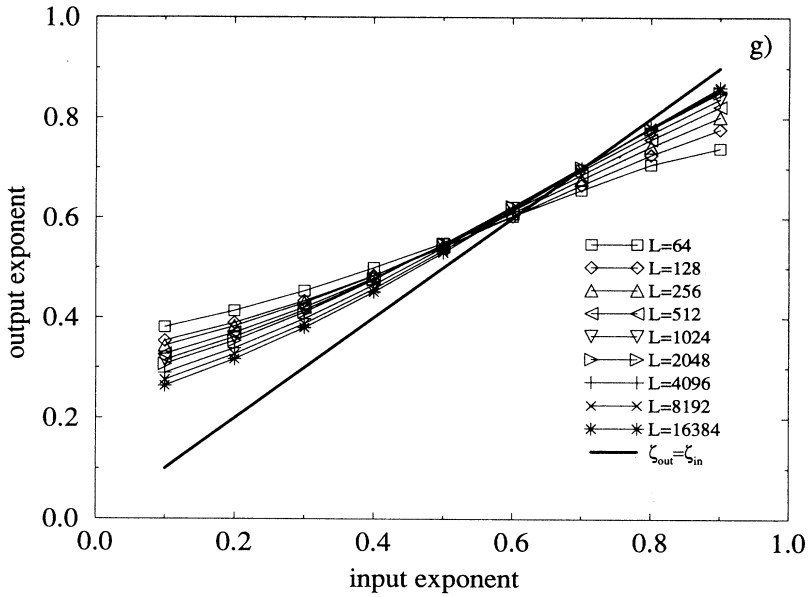

FIG. 8. (*Continued*).

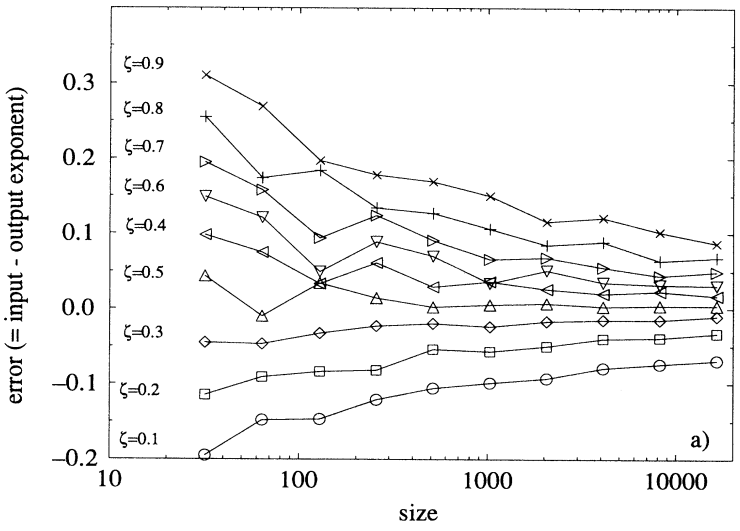

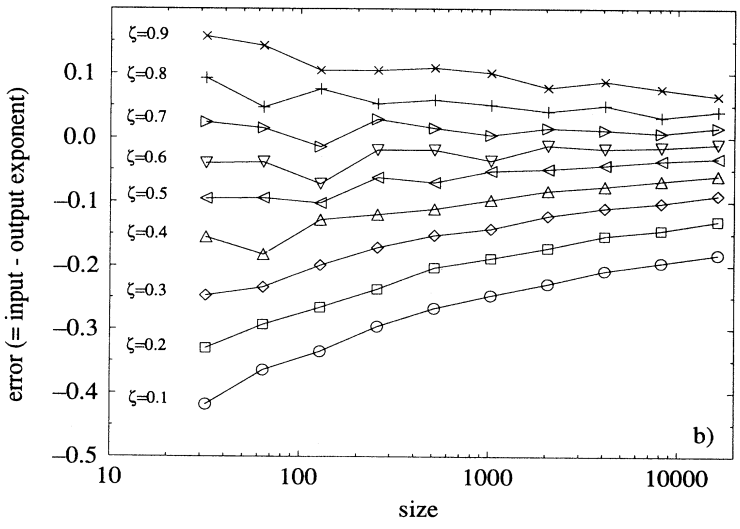

FIG. 9. Estimation of the intrinsic errors as the difference between the input exponent minus the output exponent, for the seven methods of analysis: (a) the variable bandwidth method using the rms estimator, (b) the variable bandwidth method using the maximum-minimum difference, (c) the first return probability method, (d) the multireturn probability method, (e) the power spectrum method, (f) the divider method, and (g) the box counting method. Absolute errors can be directly read from these curves.

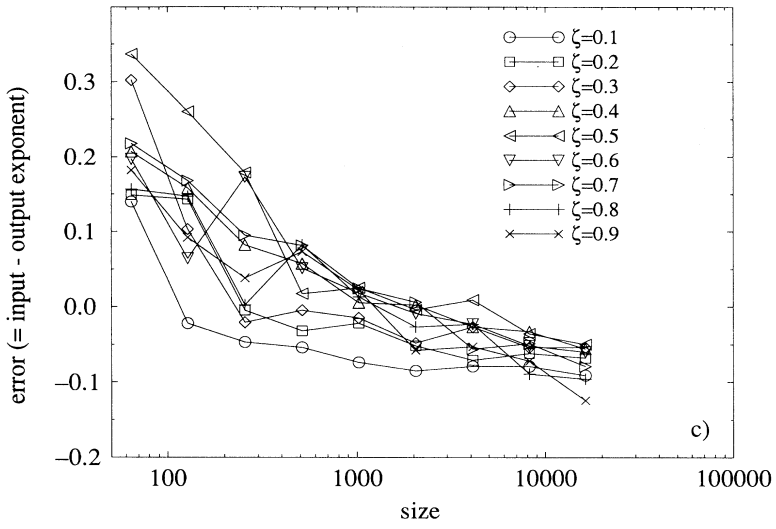

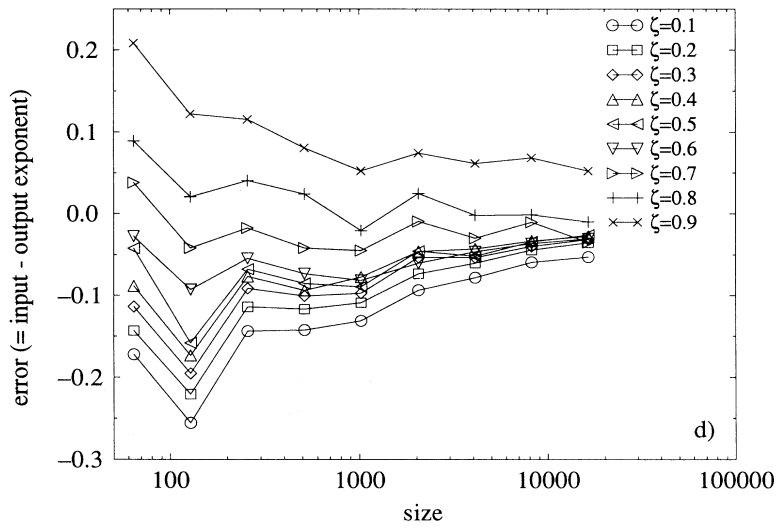

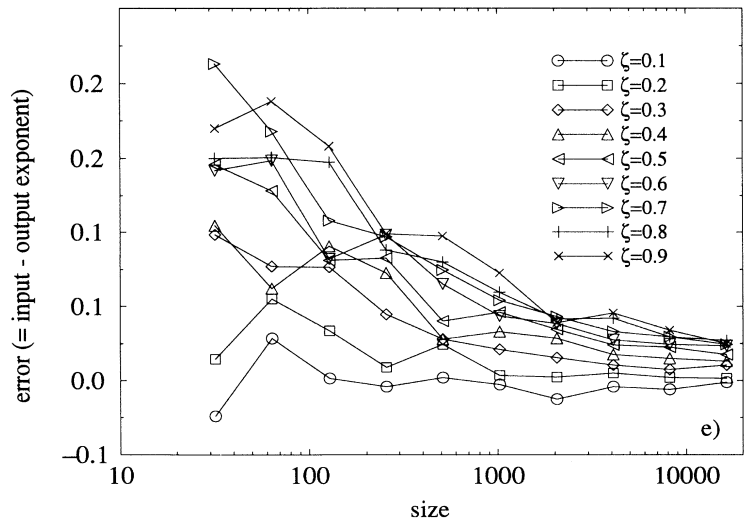

FIG. 9. (*Continued*).

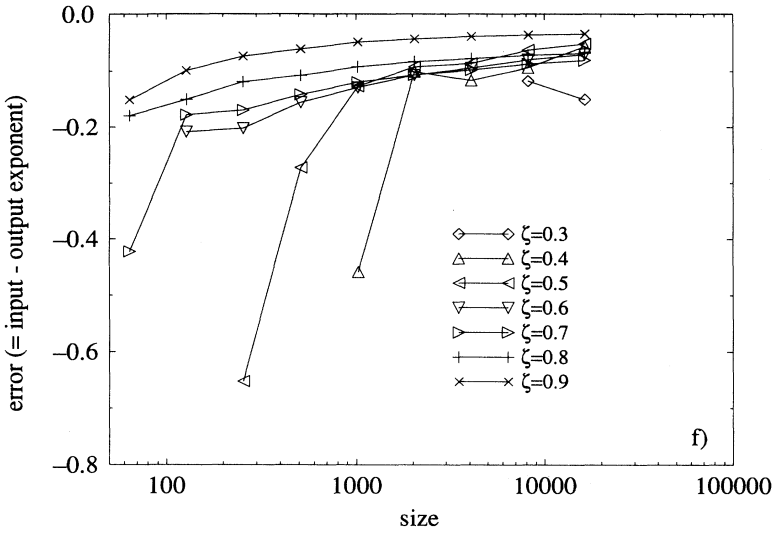

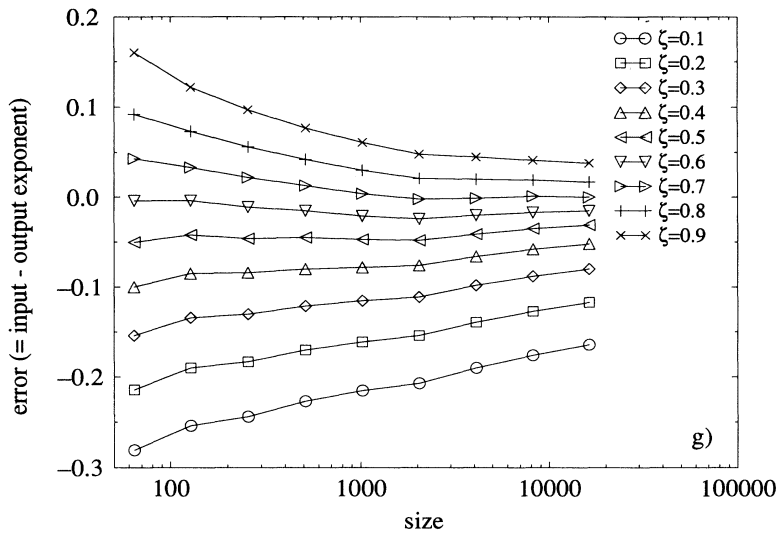

FIG. 9. (*Continued*).

9(a)–9(g) allow us to quantify the error for the different methods.

Previous effects can be also read on such figures. The role of the self-affine exponent for box counting, the rms and the maximum-minimum difference method is illustrated by well separated curves. On the contrary, the other methods (i.e., divider, first return probability, and power spectrum) provide curves more or less superimposed. There the error decreases rapidly with size. The multireturn probability can also be put in this group for a not-too-large self-affine exponent.

Absolute errors can be read directly from these curves. It supports the fact that the power spectrum method is the most reliable. The detail of the error bars are given in Table I for three typical system sizes (256, 1024, and 16 386) and for the seven methods. It is obvious from the table that a system size less than 1024 can hardly be studied seriously, unless one has some independent way of assessing the self-affine character of the profiles and a very large statistical sampling. More precise results may be extracted from the graph if a restricted range of self-affine exponents is found.

It should be emphasized that *using one single method and estimating the error bar on ζ by the quality of the power-law fit leads to a severe underestimate of the uncertainty* in all cases. Such a procedure is to be prohibited imperatively.

TABLE I. Table of error bars for all methods, for three characteristic sample sizes. The error bars are the maximum observed value for all ζ exponents. Note that these estimates may be very conservative if a narrower range of self-affine exponents is studied.

Method	$L=256$	$L=1024$	$L=16\,384$
Box	0.35	0.28	0.20
Divider	0.65	0.45	0.15
rms	0.30	0.25	0.16
Maximum-minimum	0.39	0.31	0.24
First return	0.23	0.10	0.12
Multireturn	0.25	0.18	0.10
Spectrum	0.10	0.07	0.03

VI. MEASUREMENT ARTIFACTS

Up to now the self-affine objects were assumed to be performed without any flaws. Actually, measuring a self-affine object is rather difficult and has to satisfy two main requirements. The setup has to provide a very broad dynamic (ratio between large scales and small scales) and a large sampling has to be recorded for a correct statistical description of the object. The latter point requires rapid measurement, which is difficult to combine with a broad dynamic. In this section the influence of some of the measurement errors on the self-affine analysis is assessed.

A. Large scale effects

At the system scale, the drift and the signal magnitude are the two main effects that influence the scaling analysis.

1. Misorientation

A linear drift is very often superimposed on the signal due the difficulty of determining correctly the mean plane. Adjusting the measurement setup frame to the profile frame is quite a difficult problem. In order to assess the effect of a rotation on the three methods studied above, a linear function $z=sx$ is added to the synthetic profiles.

The addition of a linear drift of slope s to a synthetic profile (which by construction has a zero mean) introduces a characteristic length scale l_c at which the typical roughness amplitude equals the linear drift

$$Al_c^{\zeta}=sl_c \ , \tag{6.1}$$

where A is the amplitude of the roughness profile. This gives the expression for the crossover scale

$$l_c \propto s^{1/(\zeta-1)} \ . \tag{6.2}$$

At scales smaller than l_c, the drift appears as a negligible correction, whereas for larger scale, the drift dominates.

Analyses of those "polluted" profiles are performed with the self-affine methods. Figures 10(a)–10(d) summarize the results obtained for a synthetic profile with exponent $\zeta=0.5$, and various slopes s. The major result

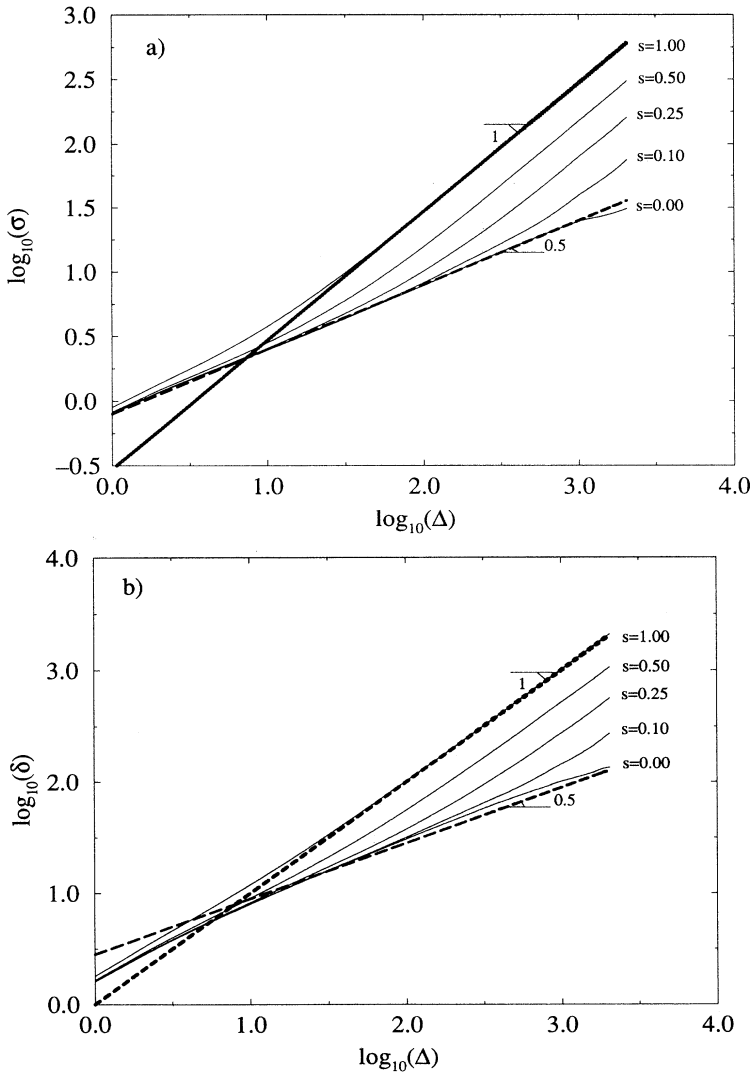

FIG. 10. Influence of an additional linear trend to the self-affine signal produced with an exponent of 0.5 for the self-affine methods: (a) the variable bandwidth method using the rms estimator, (b) the variable bandwidth method using the maximum-minimum difference, (c) the first return probability method using a logarithmic binning, and (d) the power spectrum method. The difference curves of each plot present the result of the analysis for five different values of the added slope s.

here is that all the methods are quite sensitive to the addition of a rotation. For both the rms and the maximum-minimum difference method, a linear drift introduces an apparent ζ exponent of one at large length scales. As expected, the cutoff l_c decreases as the slope s increases. One should always keep in mind that a drift may be difficult to detect for a self-affine exponent close to one and may well lead to an overestimation of that exponent. Moreover, such a unit exponent must not be misinterpreted as the signature of a self-similar object ($\zeta=1$).

The power spectrum method is also sensitive to this effect. The spectrum has a slope close to -2, which is the Fourier transform of the linear ramp. The expected slope for the power spectrum of a self-affine signal with exponent $\zeta=0.5$ turns out to be also $-1-2\zeta=-2$. Obviously one has to be cautious when such an exponent is measured from the analysis of signal. For the return probability method, the measurement is reported to be a function of s and a quantitative analysis is given in Ref. [17]. In Fig. 10(d) such an effect is not strongly pronounced.

2. *Signal amplification*

By construction, the variable bandwidth method, the return probability estimation, and the power spectrum computation are insensitive to the amplitude of the signal in terms of scaling studies. They do not couple the two directions x and z. In contrast, the divider and the box counting methods exhibit a strong sensitivity to the signal amplitude and therefore depend on the gain of the apparatus, as discussed in Sec. III.

Amplitude A plays a similar role for both methods, changing the crossover length a. The specific influence of this amplitude is shown for the divider method in Fig. 3, where three levels of the amplitude A (as previously defined) are analyzed. For a small value of A, the divider

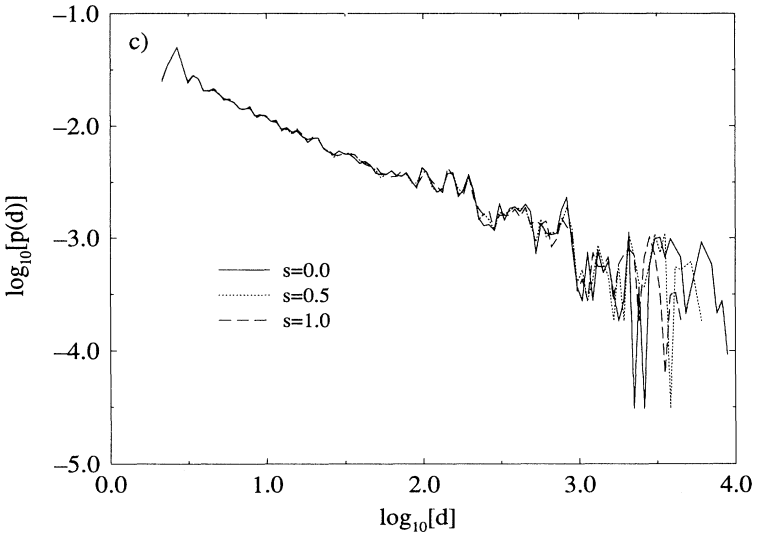

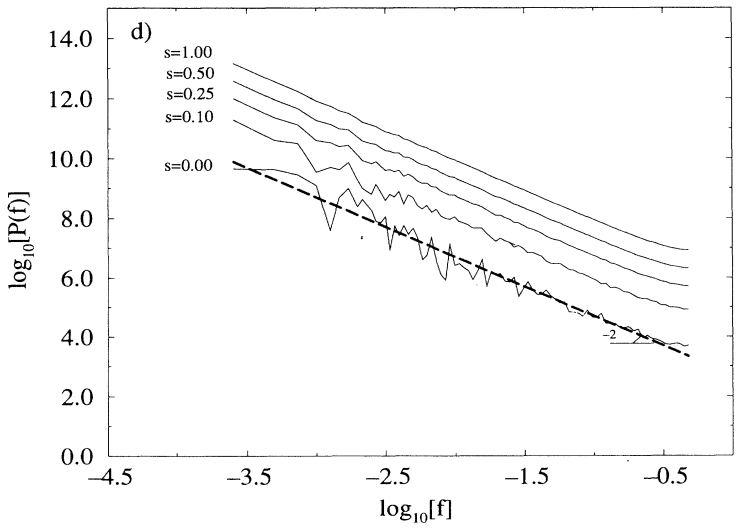

FIG. 10. (*Continued*).

just measures the horizontal length of the profile and the slope of Fig. 3 becomes one. For large amplitudes, the slope is now related to the self-affine exponent $s=-1/\zeta$.

B. Local filter

While the simple large scale artifacts discussed above can be avoided thanks to simple data filters, local filters introduce much more complicated biases. Only one example of such local filters will be studied here to illustrate the types of difficulties that may be encountered. Let us consider the measurement of a self-affine object by a mechanical tip [14]. The tip is supposed to follow slowly the profile with a given step defined here as the unit length. Due to the finite size of the needle, holes are much more difficult to reach than hills and locally the recorded geometry of the object will be partially distorted. The shape of the tip is assumed to be elliptic and characterized by two parameters: a, half of the horizontal long axis, and b, half of the vertical small axis. Two extreme cases are considered: the circle for which $a=b$ and the flat tip for which $a>b$.

Figure 11(a) shows a profile with self-affine exponent 0.8 and the tip trajectories for both geometries of the needle. A large needle is used to amplify the effects. When the tip is spherical, a path is made of circle arcs and straight lines. The number of arcs is a function of the sphere radius. On the other hand, a flat instrument reproduces more details between the tops of the hills (where a plateau appears) and the bottoms of the holes.

Power spectra are computed from these three data sets [see Fig. 11(b)]. The spectrum slope for the initial profile is well correlated to the self-affine exponent $-2.6=-1-2\zeta$. However, slopes of the "measured" profiles lead to overestimated exponents: 1.3 for the large spherical tip and 0.95 for the long flat setup. The slope s of the spectrum is a function of the needle size. In the case of a spherical tip, two extreme cases can be predicted; a zero radius—compared to the measure step—gives rise to a slope of $s=-1-2\zeta$ and a large radius leads to

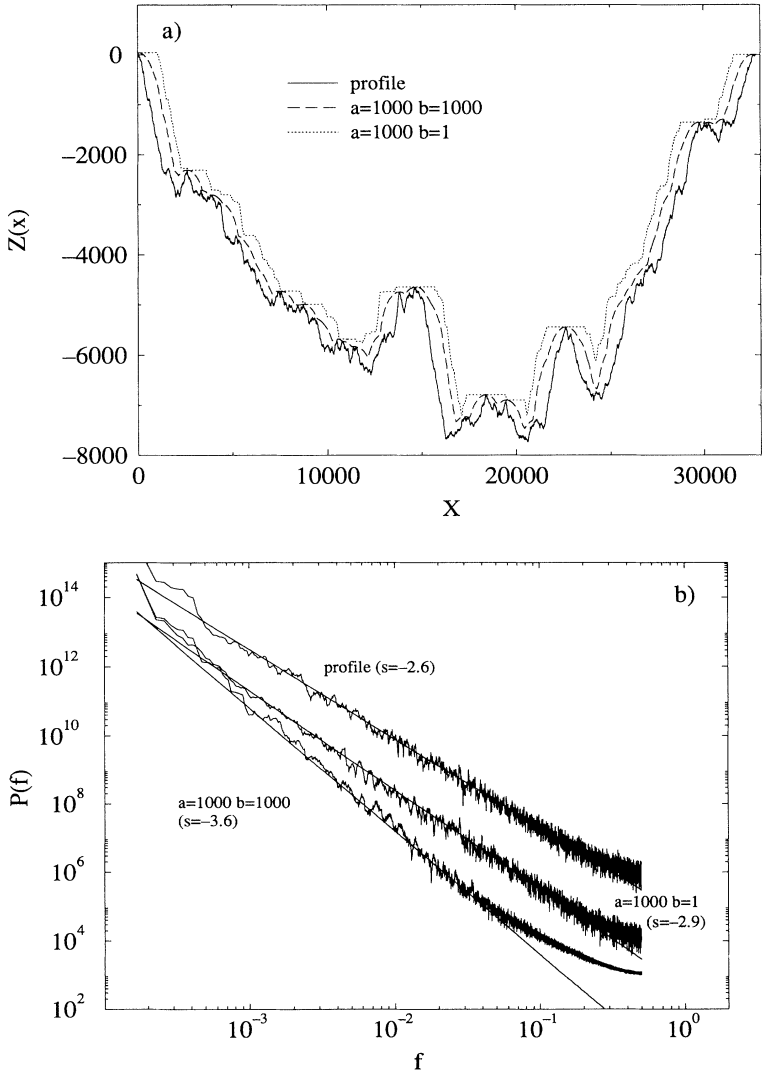

FIG. 11. Influence of a local geometric filter, due, for instance, to the tip shape of the measurement setup. An elliptic shape is assumed, with a the half horizontal long axis and b the half vertical axis. Consequently, one case corresponds to a circular tip and the other one to an almost rectangular tip. A synthetic profile with an exponent of $\zeta=0.8$ is measured using these two measurement setups. (a) The measured profiles obtained for these two cases, compared with the exact one. (b) The analysis of those biased profiles using the power spectrum method, compared with the power spectrum of the synthetic profile (with a slope of $s=-1-2\zeta$).

the description of arcs of similar radius $\zeta=2$ and $s=-4$. Even if the absolute error is wider for a flat tip, the estimation of the self-affine exponent with the Fourier spectrum is less affected.

VII. CONCLUSION

Characterization of self-affine objects is quite difficult and has to be done carefully. Two main biases in the analyses have been identified in this paper: intrinsic errors of the methods used to analyze the signal and artifacts inherent in data acquisition.

Two groups of methods can be separated. The "self-similar" methods are inherited from the so-called fractal description. We focused on the two most often used: divider and box counting. We show that a lot of care has to be taken to make them relevant. Therefore, we do not recommend them, especially the divider method. Specific "self-affine" methods have been recently developed; the variable bandwidth, the first return, and the multireturn probabilities, and the power spectrum. The intrinsic errors for the seven methods of signal analysis have been reported. For the box counting and the variable bandwidth method, the error is shown to be controlled mainly by the self-affine exponent. For the divider method, the first return and multireturn probabilities, and the Fourier spectrum, the error is shown to be controlled mainly by the finite size of the signal. For each of those methods errors have been quantified in terms of the system size and the self-affine exponent. Those results [Figs. 9(a)–9(g)] may help to assess the confidence in the measured exponents that can be expected.

There are two kinds of artifacts inherent in the geometrical description of the self-affine object: large scale filters due to a rotation or signal amplitude and local filters. Both cases can induce spurious effects which may affect the exponent determination. Careful analysis is needed to detect and filter out those effects.

All the results of this study point out that in order to estimate the reliability of a self-affine exponent, it is important to provide enough information on the apparatus used for the data recording and to systematically make use of several methods for measuring the exponent, each of those methods invoking a different response. Again we emphasize that the reliability of one single method, as judged from the quality of the power-law fit, gives a strongly underestimated value of typical error bars and thus should be avoided.

ACKNOWLEDGMENTS

We thank A. Hansen, K. J. Måløy, and F. Schmitt for useful discussions. The support of the GdR "Physique des Milieux Hétérogènes Complexes" is acknowledged.

[1] B. B. Mandelbrot, *The Fractal Geometry of Nature* (Freeman, New York, 1982).
[2] P. Meakin, Phys. Rep. **235**, 189 (1993).
[3] W. L. Newmann and D. L. Turcotte, Geophys. J. Int. **100**, 433 (1990).
[4] B. B. Mandelbrot, D. E. Passoja, and A. J. Paullay, Nature **308**, 721 (1984).
[5] E. Bouchaud, G. Lapasset, and J. Planès, Europhys. Lett. **13**, 73 (1990).
[6] S R. Brown and C. H. Scholz, J. Geophys. Res. **90**, 12 575 (1985).
[7] J. Schmittbuhl, S. Gentier, and S. Roux, Geophys. Res. Lett. **20**, 639 (1993).
[8] B. L. Cox and J. S. Y. Wang, Fractals **1**, 87 (1993).
[9] B. B. Mandelbrot, Phys. Scr. **32**, 257 (1985).
[10] S. R. Brown, Geophys. Res. Lett. **14**, 1095 (1987).
[11] Wong, in *Physics and Chemistry of Porous Media II (Schlumberger-Doll Research, Ridgefield, CT, 1986)*, Proceedings of the Second International Symposium on the Physics and Chemistry of Porous Media, AIP Conf. Proc. No. 154, edited by Jayanth R. Banavar, Joel Koplik, and Kenneth W. Winkler (AIP, New York, 1986).
[12] J. C. Charmet, S. Roux, and E. Guyon, *Disorder and Fracture* (Plenum, New York, 1990).
[13] S. Roux and A. Hansen, J. Phys. I **4**, 515 (1994).
[14] J. Schmittbuhl, F. Schmitt, and C. Scholz, J. Geophys. Res. (to be published).
[15] R. F. Voss, *Scaling Phenomena in Disorder Systems* (Plenum, New York, 1985).
[16] J. Feder, *Fractals* (Plenum, New York, 1988).
[17] A. Hansen, K. J. Måløy, and T. Engøy, Fractals (to be published).
[18] K. J. Falconer, *Fractal Geometry: Mathematical Foundations and Applications* (Wiley, Chichester, 1990).